Nanotechnology and Precision Engineering

Noise in nanopore sensors: Sources, models, reduction, and benchmarking

Cite as: Nanotechnol. Precis. Eng. 3, 9 (2020); https://doi.org/10.1016/j.npe.2019.12.008
Published Online: 23 December 2020

Shengfa Liang, Feibin Xiang, Zifan Tang, et al.

Nanotechnology and Precision Engineering 3 (2020) 9–17

Nanotechnology and Precision Engineering

Noise in nanopore sensors: Sources, models, reduction, and benchmarking

Shengfa Liang [a,b], Feibin Xiang [a,c], Zifan Tang [d], Reza Nouri [d], Xiaodong He [d], Ming Dong [d], Weihua Guan [d,e,*]

[a] Key Lab of Microelectronic Devices & Integrated Technology, Institute of Microelectronics, Chinese Academy of Sciences, Beijing 100029, China
[b] University of Chinese Academy of Sciences, Beijing 100049, China
[c] School of Electronic Electrical and Communication Engineering, University of Chinese Academy of Sciences, Beijing 100049, China
[d] Department of Electrical Engineering, Pennsylvania State University, University Park, PA 16802, United States
[e] Department of Biomedical Engineering, Pennsylvania State University, University Park, PA 16802, United States

ARTICLE INFO

Available online 29 December 2019

Keywords:
Noise
Nanopore
Model
Material
Noise reduction

ABSTRACT

Label-free nanopore sensors have emerged as a new generation technology of DNA sequencing and have been widely used for single molecule analysis. Since the first α-hemolysin biological nanopore, various types of nanopores made of different materials have been under extensive development. Noise represents a common challenge among all types of nanopore sensors. The nanopore noise can be decomposed into four components in the frequency domain (1/*f* noise, white noise, dielectric noise, and amplifier noise). In this work, we reviewed and summarized the physical models, origins, and reduction methods for each of these noise components. For the first time, we quantitatively benchmarked the root mean square (RMS) noise levels for different types of nanopores, demonstrating a clear material-dependent RMS noise. We anticipate this review article will enhance the understanding of nanopore sensor noises and provide an informative tutorial for developing future nanopore sensors with a high signal-to-noise ratio.

1. Introduction

Nanopores have emerged as a promising label-free biosensor for analyzing various kinds of biomolecules such as DNA,[1,2] RNA, and proteins.[3] A nanopore sensor is often operated by applying a constant voltage across two chambers to electrophoretically drive charged biopolymers through a nanoscale hole. The readout is an ionic current trace with individual dips corresponding to a single molecule translocation, usually called an event. The ionic current shape (*e.g.*, current blockage magnitude, shape, and duration) of each event provides the basis for interpreting the molecule length, shape, charge, and reactivity of the nanopore surface.[4–27] Various types of nanopores are currently under investigation (Fig. 1). The nanopore concept was first demonstrated with the protein pore α-hemolysin,[28] a member of the biological pore family that also includes MspA porin pores.[29] Biological nanopores have been successfully commercialized in Oxford Nanopore DNA sequencer.[30,31] In addition to the pore-forming proteins, solid-state nanopores have also been extensively studied in the past decade due to their mechanical robustness, tunable size, thermal robustness, and integration potential.[32,33] The solid-state nanopore family includes membrane materials such as SiN_x,[13,34,35] graphene,[36] glass nanopores (nanopipette),[37] and polymer nanopores.[38] While solid-state nanopores have obvious advantages over their biological counterparts due to flexibility in tuning the geometry and surface properties, the noise performance of solid-state nanopores is often worse than their biological counterparts.[39] In addition, there is a large variation in the noise of different types of nanopores.

Since the signal in the nanopore experiment is often very small, the noise represents a significant challenge that would severely limit the nanopore sensor's sensitivity and reliability. In general, the nanopore noise power spectral density (PSD) can be decomposed into 1/*f* noise, white noise, dielectric noise, and amplifier noise,[33] each dominating at different frequencies. While the nanopore noise has been extensively studied and the mechanisms previously proposed,[43–46] a systematic review and comparison of the noise performances of different nanopore types are needed.

In this work, we reviewed and summarized the physical models, origins, and reduction methods for each of these noise components. For the first time, we calculated and benchmarked the root mean square (RMS) values for different types of nanopores. There is a clear material-dependent intrinsic nanopore noise performance. The correlation of the noise performance to the nanopore materials may provide

* Corresponding author at: Department of Electrical Engineering, Pennsylvania State University, University Park, PA 16802, United State.
E-mail address: w.guan@psu.edu (W. Guan).

https://doi.org/10.1016/j.npe.2019.12.008

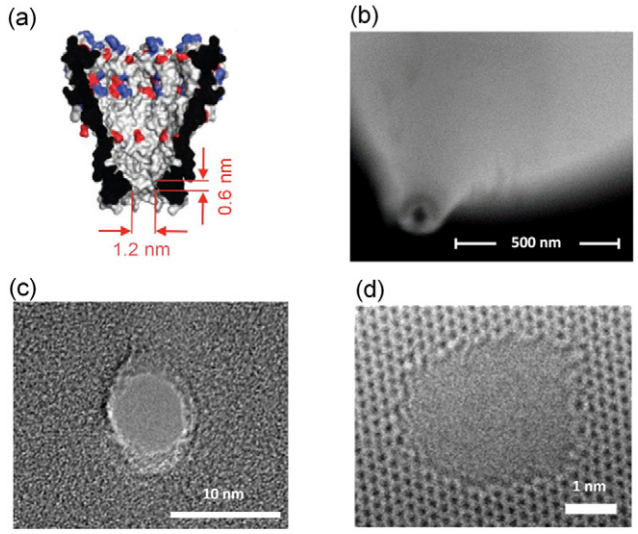

Fig. 1. Structures of different nanopore types. (a) MspA protein nanopore[40] (Reprinted by permission from [Springer Nature Customer Service Centre GmbH]: [Springer Nature] [Nature Biotechnology] (Reading DNA at single-nucleotide resolution with a mutant MspA nanopore and phi29 DNA polymerase, Manrao EA et al.), [COPYRIGHT] (2012)). (b) Glass nanopore[41] (Reprinted with permission from [Nouri R, Tang ZF, Guan WH. Calibration-free nanopore digital counting of single molecules. *Analytical Chemistry* 2019;91(17):11178-11184.]. Copyright (2019) American Chemical Society.). (c) SiN_x nanopore. (d) Graphene nanopore[42] (Reprinted by permission from [Springer Nature Customer Service Centre GmbH]: [Springer Nature] [Nature Communications] [Tailoring the hydrophobicity of graphene for its use as nanopores for DNA translocation, Schneider GF et al.], [COPYRIGHT] (2013)).

alternative insight into understanding and controlling the nanopore noise. We anticipate this review article would provide an informative tutorial into developing future nanopore sensors with improved signal-to-noise ratio (SNR).

2. Nanopore noise analysis and model

There are generally two approaches for analyzing the nanopore noise. One approach is to directly calculate the RMS value in the time domain,[47–49]

$$I_{\mathrm{rms}} = \sqrt{\overline{\Delta I^2(t)}} \tag{1}$$

where $\Delta I(t)$ represents the fluctuation of the current $I(t)$ deviating from its mean value.

The RMS current can be directly compared to the molecule translation signal for evaluating the SNR,[50]

$$\mathrm{SNR} = \Delta I_{\mathrm{ionic}}/I_{\mathrm{rms}} \tag{2}$$

where $\Delta I_{\mathrm{ionic}}$ represents the current blockage amplitude when the charged biopolymers pass through the nanopore.

The other approach is frequency domain analysis of the PSD,[51] which can be derived as,

$$S_I(f) = \frac{1}{2T}\lim_{T\to\infty}\left|\int_{-T}^{T}\Delta I(t)\mathrm{e}^{-2\pi ift}\mathrm{d}t\right|^2 \tag{3}$$

The noise RMS can be related to the noise PSD as,

$$I_{\mathrm{rms}} = \mathrm{sqrt}\left(\int_{f1}^{f2} S_I(f)\mathrm{d}f\right) \tag{4}$$

Generally, the noise PSD can be decomposed into four components as,

$$S_I(f) = S_{\mathrm{F}}(\propto 1/f) + S_{\mathrm{W}}\left(\propto f^0\right) + S_{\mathrm{D}}(\propto f) + S_{\mathrm{A}}\left(\propto f^2\right) \tag{5}$$

where f is the frequency; S_{F}, S_{W}, S_{D}, and S_{A} represent the PSD of $1/f$ noise, white noise, dielectric noise, and amplifier noise, respectively.[33]

Fig. 2(a) summarizes the general characteristics of the nanopore noise PSD.[50] At low frequencies, noise PSD is mainly contributed to by the $1/f$ noise. At moderate frequencies, dielectric noise due to dielectric thermal loss starts to become a major source of the noise. At high frequencies, noise is dominated by the amplifier noise. The white noise is spread uniformly at different frequencies and could be overwhelmed by the $1/f$ and dielectric noise, while being unaffected by the noise PSD.[44,52] The transition points where each noise source starts to dominate could vary tremendously among different experiments.[39,52–54] Fig. 2(b) shows the equivalent circuit model for describing the noise component in the nanopore sensors.[55] In Sections 3 to 6, we review and summarize the general characteristics of each of these noises and discuss approaches for noise reduction.

3. 1/*f* noise

3.1. 1/*f* noise origin

A widely accepted theory of $1/f$ noise is that its spectra consists of a set of Lorentzian noises that come from a group of random telegraph noises (RTNs).[56] This model was verified by magnetization current experiments.[57] Specifically, the observed $1/f$ noise is the superposition of many discrete RTNs. $1/f$ noise often dominates the total noise at frequencies <1 kHz and is the most widely studied.[39,51,58,59]

The exact origin of the $1/f$ noise remains controversial. A variety of $1/f$ noise mechanisms have been proposed, including the channel's opening-closing process,[60] structural flexibility of the nanopore pore walls,[61] nanobubbles,[62,63] incomplete hydrophilicity of the nanopore surface,[64] cooperative fluctuations on ion motion along a confined space,[65] surface reversible adsorption of ions combined with the ions' long-lasting excursions in the reservoirs,[66] carbon contaminants surrounding the nanopore surface during transmission electron microscopy (TEM) drilling,[67] and mechanical vibrations.[68–72] These mixed models strongly indicate the $1/f$ noise stems from many different sources.

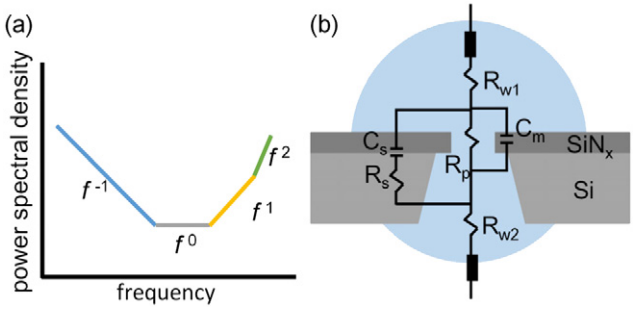

Fig. 2. Noise PSD distribution and equivalent circuit of the nanopore. (a) Noise PSD on a log-log scale (redrawing based on reference[50]) (Reprinted from Analytica Chimica Acta, 1061, Hartel AJW et al., High bandwidth approaches in nanopore and ion channel recordings - A tutorial review, 13–27, Copyright (2019), with permission from Elsevier.). (b) Structure of simplified model circuits of the pores (redrawing based on reference[55]) (Reprinted with permission from [Waggoner PS, Kuan AT, Polonsky S, Peng HB, Rossnagel SM. Increasing the speed of solid-state nanopores. *Journal of Vacuum Science & Technology B* 2011;29(3):032206.]. Copyright [2011], American Vacuum Society.). Here R_{w1} and R_{w2} are the resistance between the electrodes and electrolytes. R_{p} represents the resistance of the pore structure. R_{s} represents the electrical path between the substrate and the dielectric layer. C_{s} and C_{m} are the substrate capacitance and suspended membrane capacitance.

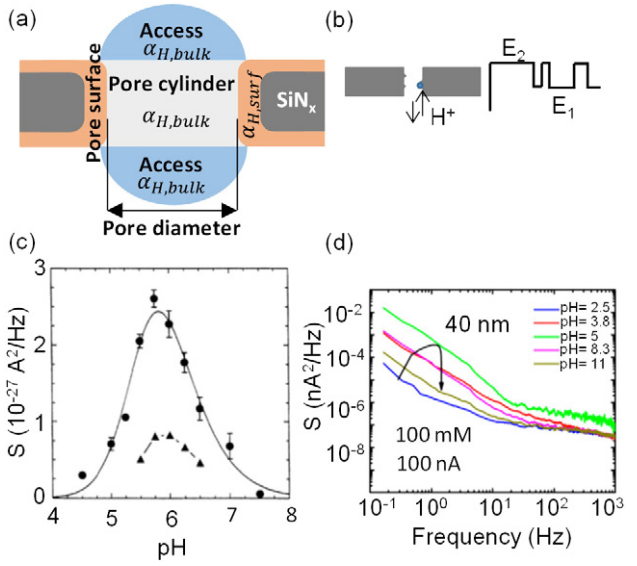

Fig. 3. Sources of noise distribution in a nanopore and surface effect on *1/f* noise. (a) Scheme of a solid-state nanopore (redrawing based on reference[59]) (Republished with permission of Nanotechnology, from [*1/f* noise in solid-state nanopores is governed by access and surface regions, Fragasso A et al., 30, 395202 2019]; Permission conveyed through Copyright Clearance Center, Inc.). (b) Simple model of a reversible ionization reaction of groups on the surface of a nanopore channel (redrawing based on reference[73]); Surface charge effect on PSD of different nanopores: (c) Biological nanopore[73] (Reprinted figure with permission from [Bezrukov SM et al., Physical Review Letters, 70, 2352–2355 1993.] Copyright (1993) by the American Physical Society.). (d) Solid-state nanopore (SiN_x nanopore)[74] (Reprinted with permission from [Wen C, Zeng SS, Arstila K, et al. Generalized noise study of solid-state nanopores at low frequencies. *ACS Sensors* 2017;2(2):300–307.]. Copyright (2017) American Chemical Society.).

Among all of the existing models for 1/*f* noise, the most widely studied is the conductance fluctuation model. To understand this model, the nanopore structure is divided into three parts, the pore-surface, pore-cylinder, and access region,[59] as shown in Fig. 3(a). The whole nanopore resistance can be modeled as,[59]

$$R_{\mathrm{tot}} = R_{\mathrm{access}} + \left(R_{\mathrm{p,bulk}} // R_{\mathrm{p,surf}}\right) \tag{6}$$

in which ($R_{\mathrm{p,\ bulk}}//R_{\mathrm{p,\ surf}}$) represents the channel resistance (R_{pore}) in the nanopore; the "//" symbol means the parallel connection of the two resistors; R_{access} is the nanopore access resistance. The 1/*f* noise PSD can, therefore, be expressed as,[59]

$$S_{I,\mathrm{tot}} = \frac{V^2}{f R_{\mathrm{tot}}^4}\left[\frac{\alpha_{\mathrm{H,bulk}} R_{\mathrm{access}}^2}{N_{\mathrm{access}}} + \left(\frac{\alpha_{\mathrm{H,bulk}}}{R_{\mathrm{p,bulk}}^2 N_{\mathrm{p,bulk}}} + \frac{\alpha_{\mathrm{H,surf}}}{R_{\mathrm{p,surf}}^2 N_{\mathrm{p,surf}}}\right) R_{\mathrm{pore}}^4\right] \tag{7}$$

in which $\alpha_{\mathrm{H,\ bulk}}$ is the bulk Hooge constant and $\alpha_{\mathrm{H,\ surf}}$ is the surface Hooge constant; N_{access}, $N_{\mathrm{p,\ bulk}}$ and $N_{\mathrm{p,\ surf}}$ are the charge carrier numbers in the access, pore-cylinder, and pore-surface region, respectively. Based on the conductance fluctuation model (Eq. (7)), the 1/*f* noise can be attributed to the fluctuation of the surface and bulk conductance. In the following section, we will separately discuss these two effects.

3.1.1. Surface effect

Surface charges exist at the nanopore walls[46,73,75] and their fluctuation may induce the surface conductance change in the nanopore. Fig. 3 (b) shows a simple model of a reversible ionization reaction on the nanopore wall surface. In this model,[73] E_1 and E_2 represent two different energy states at a single point on the nanopore walls, which corresponds to the association and dissociation of the protons. The probability of state E_1 and E_2 were given by,

$$P_1 = \frac{\tau_1}{\tau_1 + \tau_2} = \frac{1}{1 + 10^{pK - pH}}, P_2 = 1 - P_1 \tag{8}$$

Here, *pK* represents the log form of the equilibrium constant; *pH* represents the measure of the acidity or basicity of a solution; τ_1 and τ_2 represent the mean time spent in states E_1 and E_2, respectively. The PSD of the Lorentzian RTN noise associated with site *j* can be represented as,

$$S_j(f) = \frac{4\left(\Delta i_{1,2}\right)^2 \tau^2}{(\tau_1 + \tau_2)\left[1 + (2\pi f\tau)^2\right]} \tag{9}$$

in which $\tau = \tau_1 * \tau_2/(\tau_1 + \tau_2)$. For sufficiently large numbers of RTN noise, a macro 1/*f* spectrum could appear.[56] A previous molecular dynamics (MD) simulation demonstrated excellent agreement to the adsorption-desorption model predictions.[66]

The surface charge fluctuation can be affected by the pH,[73,74] ionic concentration,[46] and film material.[51] From the perspective of pH, Fig. 3 (c) and (d) show the nanopore PSD under different pH values, for biological and SiN_x nanopores, respectively. Both PSDs showed the same trend with pH; the peak PSD appears at intermediate pH values, corresponding to the material's point of zero charges. From the perspective of ionic concentration, the normalized PSD (S_G/G^2) increases with decreasing concentrations[44,46] as the nanopore size is comparable to or even smaller than the Debye length at low ionic concentrations. As a result, ions in the nanopore will be more significantly affected by surface charge fluctuations. From the perspective of the material, the different materials have different surface functional groups with varying densities of charges. As a result, nanopores made of different materials will have different 1/*f* noise properties.[51] For example, the 1/*f* noise of a SiN_x nanopore is usually much larger than that of a biological nanopore[39] or glass nanopore.[76]

Hydrophilicity is another important surface effect that could affect the 1/*f* noise. It was previously hypothesized that nanobubbles can form at a nanopore surface that produces high 1/*f* noises when the surface is hydrophobic.[62,63]

3.1.2. Bulk effect

The bulk and access region of the nanopore is another important source for the 1/*f* noise (Eq. (7)).[59] The bulk effect mostly comes from ionic mobility fluctuation. The mobility fluctuation can be caused by (1) ionic crowding due to larger ion concentrations in the pore under a voltage bias for a single rectifying conically-shaped nanopore; (2) electrostatic interactions between passing ions and pore walls; and (3) vortices formations at the pore entrance due to the conical geometry.[77] The exact mechanism remains unclear, as illustrated by a variety of models. For example, Fragasso et al. ascribed the carrier free path length fluctuations as the origin for ion mobility fluctuations.[59] Tasserit et al. hypothesized the confinement-induced cooperative fluctuation of ion mobility leads to 1/*f* noise.[65] The ionic concentration and nanopore geometry will also affect the mobility fluctuations. Wen et al. argued that the bulk region of the nanopore structure plays a dominant role in noise at high concentrations.[74]

3.2. Reducing the 1/f noise

For surface-related 1/*f* noise sources, improvements in the hydrophilicity are the most common practice (Fig. 4), which can be achieved by atomic layer deposition (ALD) of TiO_2[78] or Al_2O_3[79] (Fig. 4(a) and (b)), piranha cleaning,[39] oxygen plasma,[39] and pulsed voltage treatment[64] (Fig. 4(c)). Among these methods, ALD deposition is capable of reducing the surface charge density, which can also be achieved by changing the pH. Finally, using alternative nanopore materials[76] (Fig. 4(d)) can also reduce the surface-related 1/*f* noise.

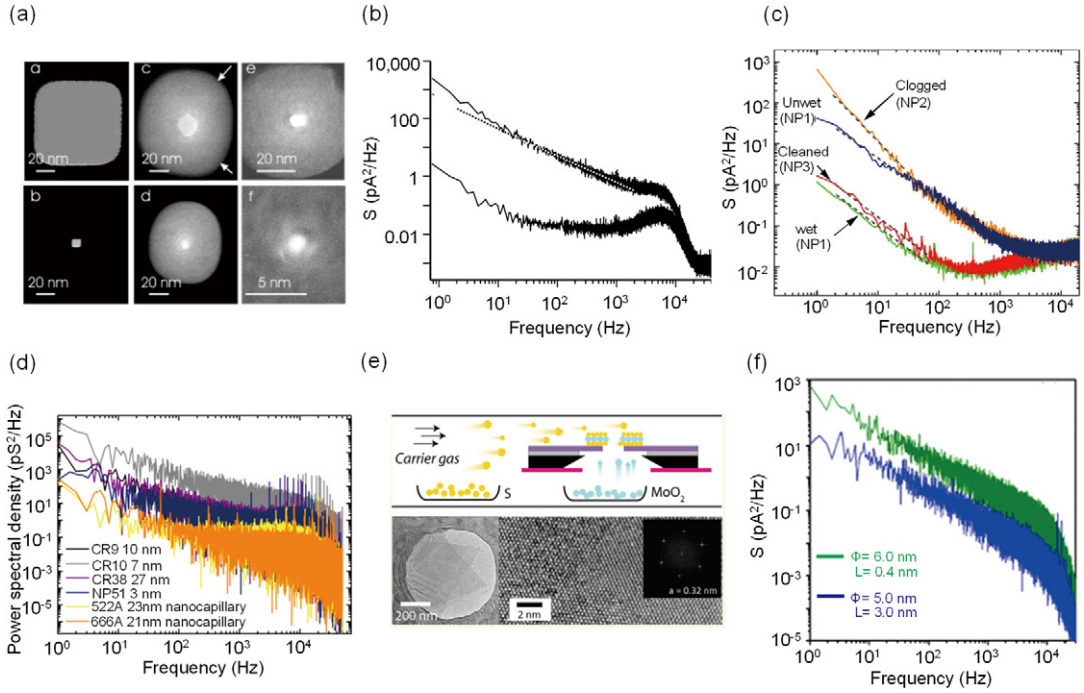

Fig. 4. Methods for reducing 1/*f* noise. (a) Depositing Al_2O_3 by ALD and (b) reducing effect, here the higher line represents an untreated chip and the lower line represents a treated chip[79] ((a) and (b) reprinted with permission from [Chen P, Mitsui T, Farmer DB, Golovchenko J, Gordon RG, Branton D. Atomic layer deposition to fine-tune the surface properties and diameters of fabricated nanopores. *Nano Letters* 2004;4(7):1333–1337.]. Copyright (2004) American Chemical Society.). (c) Hydrophilic treatment using a "zapping" method[64] (Republished with permission of Nanotechnology, from [Precise control of the size and noise of solid-state nanopores using high electric fields, Beamish E et al., 23, 405301 (7pp) 2012]; Permission conveyed through Copyright Clearance Center, Inc.). (d) Power spectral density comparing between glass and SiN_x nanopore[76] (Reprinted with permission from [Steinbock LJ, Bulushev RD, Krishnan S, Raillon C, Radenovic A. DNA translocation through low-noise glass nanopores. *ACS Nano* 2013;7(12):11255–11262.]. Copyright (2013) American Chemical Society.). (e) Direct and scalable deposition of low-noise MoS_2 membranes by a CVD method[80] (Reprinted with permission from [Waduge P, Bilgin I, Larkin J, et al. Direct and scalable deposition of atomically thin low-noise MoS_2 membranes on apertures. *ACS Nano* 2015;9(7):7352–7359.]. Copyright (2015) American Chemical Society.). (f) Comparison of the noise power spectrum density of single- and multi-layer graphene nanopores[68] (Republished with permission of Nanotechnology, from [Noise and its reduction in graphene-based nanopore devices, Kumar A et al., 24, 495503 (7pp) 2013]; Permission conveyed through Copyright Clearance Center, Inc.).

For bulk-related 1/*f* noise sources, decreasing the mobility fluctuation can be achieved by increasing the concentration of electrolyte or by choosing nanopores with a large pore diameter. The bulk-related 1/*f* noise can be improved by enhancing the film mechanical stability (Fig. 4(e)),[80] increasing the film thickness (Fig. 4(f)),[68] and decreasing the film free-standing area.[71] Enhancing the film mechanical stability is of particular importance to reducing the noise of 2D material nanopores.

4. White noise

4.1. White noise origin

A key characteristic of white noise is the PSD is independent of the frequency. There are two sources for the white noise, thermal noise, and shot noise.[59] The general white noise can be written as,

$$S_{I,\text{white}} = S_{I,\text{thermal}} + S_{I,\text{shot}} = 4KTG + 2qI \tag{10}$$

where G is the conductance, K is the Boltzmann constant, T is the temperature, q is the elementary charge, and I is the current. The thermal noise (Johnson noise) arises from thermal fluctuations in the charge carriers (*i.e.*, ions in the nanopore sensors). The shot noise (Poisson noise) normally occurs when there is a potential barrier. In the nanopore sensors, the Ag/AgCl interface is an example of a potential barrier. When the electrons/ions cross that barrier, shot noise can be produced.[43] Note that a pure resistor normally does not produce shot noise since there is no potential barrier. Both thermal and shot noises are inherent to a real system, representing fundamental limitations (lower noise floor) in making sensitive measurements.

4.2. Reducing the white noise

One possible method to decrease the thermal noise is to decrease the conductance by decreasing the charge carriers' concentration or the pore size.[43] Increasing the channel length of the nanopore could also decrease the thermal noise, however, this would reduce the sensitivity of the pore.[81]

5. Dielectric noise

5.1. Dielectric noise origin

Dielectric noise is related to dielectric loss due to the non-ideal existence of charge carriers in the dielectric material.[43] In nanopores, while the measured current is exclusively from the ionic current through the nanopore, there is always a leakage current through the non-ideal dielectric membrane (in which charge carriers exist). The thermal fluctuations of this non-ideal leakage current contribute to dielectric noise. To study the dielectric noise induced by non-ideal capacitance C_n, it can be modeled as an ideal capacitor C_i in parallel with admittance Y_f related to the dielectric loss (Fig. 5(a)). Therefore, the dielectric noise can be described as,

$$S_D(f) = 4kT{\cdot}Y_f = 8\pi kTC_nD{\cdot}f \tag{11}$$

where D is the dielectric loss constant. It is clear that material with more loss will have greater dielectric noise.

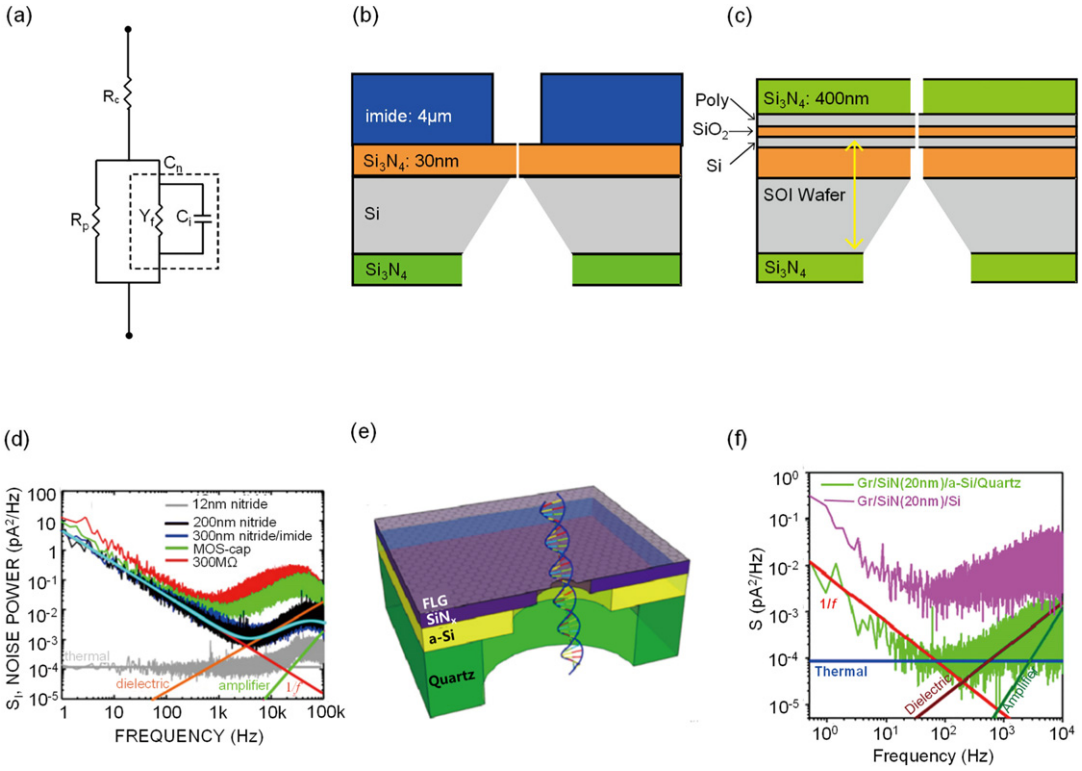

Fig. 5. Model and reduction of dielectric noise. (a) Equivalent circuit model based on Fig. 2(b) for dielectric noise. R_c ($=R_{w1}+R_{w2}$) is the resistance of two electrolyte cells. R_p is the resistance from the nanochannel. C_n represents the non-ideal membrane capacitance, which is the sum of C_m and C_s and is expressed in parallel connection of an admittance Y_f and an ideal capacitance C_i. (b) A SiN_x chip was coated by polyimide. (c) Polysilicon/SiO_2/Si (MOS), a multiple-layer structure, was used for nanopore fabrication. (d) The PSD of four different structures, two of which are shown in (b) and (c). (b-d) Redrawing based on reference[52] (Republished with permission of Nanotechnology, from [Nanopores in solid-state membranes engineered for single molecule detection, Dimitrov V et al., 21, 065502 (11pp) 2010]; Permission conveyed through Copyright Clearance Center, Inc.). (e) Schematic of a graphene chip with quartz substrate, connected by a thin Si layer. (f) Noise power spectrum density of two chips with Si or quartz substrate. (e-f) Redrawing based on reference[68] (Republished with permission of Nanotechnology, from [Noise and its reduction in graphene-based nanopore devices, Kumar A et al., 24, 495503 (7pp) 2013]; Permission conveyed through Copyright Clearance Center, Inc.).

5.2. Reducing dielectric noise

Based on Eq. (11), the dielectric noise is determined by the total capacitance and dielectric loss constant of the material that isolates the electrolyte. Therefore, two clear approaches can be used to reduce the dielectric noise. One is to reduce the total capacitance, which can be done by covering the nanopore chip with insulation materials (*e.g.*, PDMS[39] and polyimide[52]). Stacked dielectric structures can also be used.[53,82] With these methods, the dielectric noise was reduced by 1–2 orders of magnitude, as shown in Fig. 5(b)–(d). The other approach is to use materials with less loss. Since the Si substrate is often the main source of the dielectric loss, another insulation material can be deposited on the substrate or another substrate can be used. It was experimentally observed that the biological and glass nanopores, in general, have better dielectric noise performances than SiN_x and 2D material nanopores, which can be attributed to the latter's high loss factor from the Si substrate. Kumar[68] used quartz as the substrate of graphene nanopores (Fig. 5(e)) and the dielectric noise was significant decreased (Fig. 5(f)). Other materials, such as Telflon[54] and polyimide,[83] can also be used to replace Si. Clearly, the dielectric noise can be reduced by combining these two approaches. For example, de Vreede[84] nearly completely suppressed the dielectric noise at a wide bandwidth (<100 kHz) using a fused silica substrate and covering it with PDMS.

6. Amplifier noise

6.1. Amplifier noise origin

In a high-frequency range, the noise PSD is proportional to f^2, corresponding to the amplifier noise. The amplifier noise comes from the interactions of thermal noise at the amplifier input and the total capacitance in the system (including capacitances from the chip and the amplifier).[53] The amplifier noise can be expressed as,[33]

$$S_A(f) = (2\pi C_t e_n)^2 \cdot f^2 \tag{12}$$

in which e_n is the voltage thermal noise, C_t is the total capacitance that consists of the nanopore capacitance (C_i), feedback capacitance (C_f), and other parasitic capacitance (C_p), as shown in Fig. 6(a).

6.2. Reducing amplifier noise

According to Eq. (12), the amplifier noise is determined by the total capacitance C_t and voltage thermal noise, e_n. Reducing the C_t is a common practice to suppress the amplifier noise, which can be realized two ways. One is to reduce the nanopore capacitance. For example, replacing the intrinsic SiN_x nanopore (C_i = 48.6 pF) with a glass-passivated nanopore chip with C_i < 10 pF[82] (Fig. 6(b)) can greatly reduce the amplifier noise (Fig. 6(c)). The other way is to use amplifiers with low parasitic capacitance (C_p and C_f) as well as reduced voltage thermal noise. For example, replacing the commonly used Axopatch 200B with a CMOS integrated nanopore platform (CNP) (Fig. 6(d))[53] is effective in reducing the amplifier noise (Fig. 6(e) and (f)).

7. Material-dependent RMS noise benchmarking

Among the four noise components we discussed, the *1/f* and dielectric noise are intrinsic to nanopore materials. To benchmark the noise levels of different materials, we summarized the RMS noise level for biological (Table 1), quartz glass (Table 2), SiN_x (Table 3), and 2D material

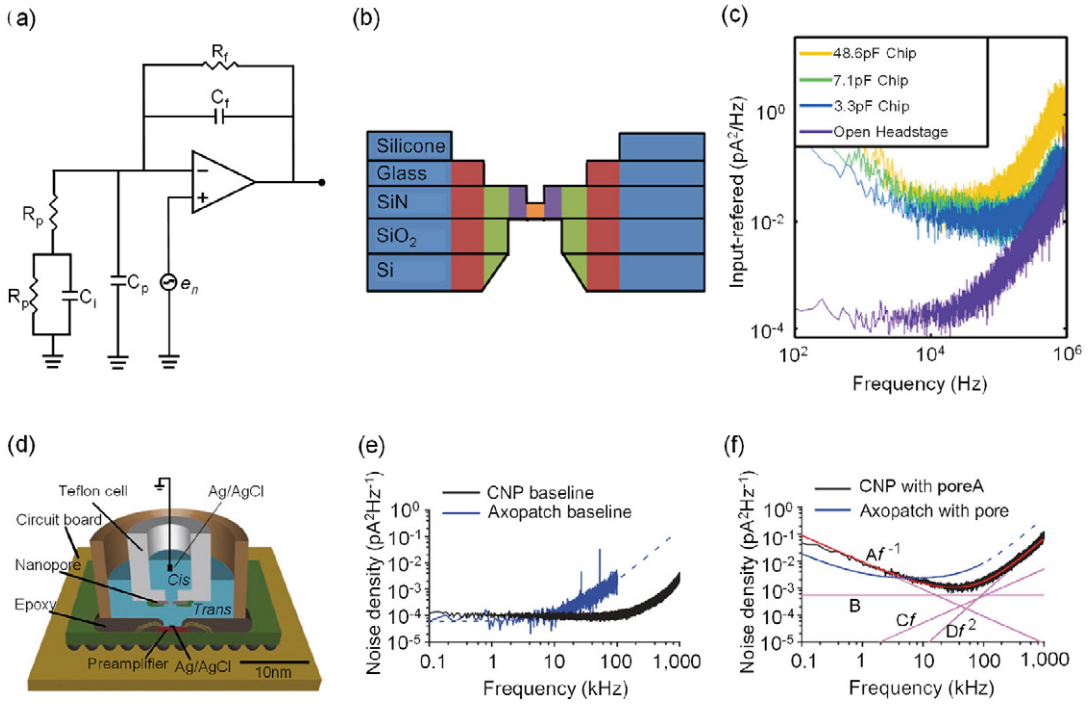

Fig. 6. Model and reduction for amplifier noise. (a) Equivalent circuit model based on Fig. 2(b) for the calculation of amplifier noise. R_c, R_p, and C_i have the same meaning with symbols in Fig. 5(a). R_f is the feedback resistance. (b) Schematic diagram of a glass-passivated nanopore chip. (c) Comparison of power spectra density of two glass-passivated chips (3.3 pF and 7.1 pF) and a non-passivated chip (48.6 pF). (b–c) Redrawing based on reference[82] (Reprinted with permission from [Balan A, Machielse B, Niedzwiecki D, et al. Improving signal-to-noise performance for DNA translocation in solid-state nanopores at MHz bandwidths. *Nano Letters* 2014;14(12):7215–7220.]. Copyright (2014) American Chemical Society.). (d) Schematic diagram of the measurement setup of CNP platform. (e) Comparison of the baseline noise spectrum of a similar open-headstage configuration connecting with CNP and Axopatch 200B. (f) Comparison of the noise power spectra of nanopores when tested by CNP and Axopatch 200B. (d–f) Redrawing based on reference[53] (Reprinted by permission from [Springer Nature Customer Service Centre GmbH]: [Springer Nature] [Nature Methods] (Integrated nanopore sensing platform with sub-microsecond temporal resolution, Rosenstein JK et al.), [COPYRIGHT] (2012)).

(Table 4) nanopores. The I_{rms} values in Tables 1–4 were calculated from the reported PSD data using Eq. (4), or based on the reported I_{rms} data acquired directly from the text or chart, within the same bandwidth from 1 Hz to 10 kHz for a fair comparison. Fig. 7 shows the RMS noise scattering plot as a function of the nanopore materials. The noise level in the SiN_x nanopore and 2D material nanopore is greater than that in the glass nanopore, while the biological nanopores show the best noise performance. The two populations in the quartz glass nanopore

Table 1
Noise level statistic of biological nanopores.

Structure	I_{rms} (pA)	Diameter (nm)	Ionic strength (Molar)	pH	Bias (mV)	Ref.
α-Hemolysin	2.70	n.a.	1.00	8.00	200	39
	2.51	1.4	0.20	7.40	100	86
	2.49	1.4	0.20	7.40	0	86
	4.47	1.4	1.00	3.50	100	86
	2.13	1.4	1.00	3.50	0	86
FhuA ΔC/Δ4L	2.69	3.1–4.4	0.20	7.40	100	86
	2.49	3.1–4.4	0.20	7.40	0	86
	2.13	3.1–4.4	1.00	3.50	0	86
ClyA	2.08	3.8	0.15	7.50	35	87
	2.07	3.8	0.15	7.50	−35	87
	2.07	3.8	0.15	7.50	0	87

Table 2
Noise level statistic of quartz-based glass nanopores.

Structure	I_{rms}(pA)	Diameter (nm)	Ionic strength (Molar)	pH	Bias (mV)	Ref.
Bare nanopore	3.09	25.0	0.001	n.a.	−500	88
	1.79	75.0 ± 5.0	1.00	8.0	300	85
	27.06	21.0	1.00	8.0	2000	76
	24.90	23.0	1.00	8.0	2000	76
Au deposited	2.91	15.0	0.001	n.a.	−500	88
Al_2O_3 deposited	17.35	59.0 ± 5.0	1.00	8.0	300	85
	16.72	47.0 ± 5.0	1.00	8.0	300	85
	20.11	41.0 ± 5.0	1.00	8.0	300	85

Table 3
Noise level statistic of SiN_x nanopores.

Structure	I_{rms} (pA)	Diameter (nm)	Ionic strength (Molar)	pH	Bias (mV)	Ref.
Bare SiN_x	45.58	n/a	1.00	8.0	200	39
	63.20	20.0	1.00	8.0	100	89
	48.10	20.0	1.00	8.0	100	89
	90.47	20.8	1.00	7.5	100	44
	27.07	22.0	1.00	7.5	100	44
	147.00	n/a	1.00	8.0	0	83
	27.10	3.3–4.0	1.00	8.0	100	52
	131.60	n/a	1.00	8.0	4.5 (nA)[a]	54
	38.00	n/a	1.00	8.0	0	54
	21.90	n/a	1.00	8.0	200	39
	28.60	7.0	1.00	8.0	200	64
Bare SiN_x with zapping treatment	13.60	7.0	1.00	8.0	200	64
	14.40	21.0	1.00	8.0	200	64
PDMS coated	6.45	n/a	1.00	8.0	200	39
PI coated	6.40	1.7–2.8	1.00	8.0	100	52
MOS-cap[b]	6.40	7.1–7.3	1.00	8.0	100	52
SiO_2 coated	33.10	20.0	1.00	8.0	100	89
	24.50	20.0	1.00	8.0	100	89
	28.30	20.0	1.00	8.0	100	89
Stacked	7.11	n/a	1.00	8.0	n/a	53
Glass-passivated stacked	16.37	n/a	1.00	8.0	n/a	82
	23.36	n/a	1.00	8.0	n/a	82
PI substrate	5.40	n/a	1.00	8.0	0	83
Quartz substrate	12.58	n/a	1.00	8.0	4.5 (nA)[a]	54

[a] Driven by constant current.
[b] MOS-cap means the SiN_x membrane was replaced by a MOS structure.

were mainly due to (1) the difference between the bare nanopore and surface-coated nanopores,[85] and (2) the different experimental conditions.

Material-related RMS noise is related to the 1/*f* noise and dielectric noise dominating the total noise. From the 1/*f* noise perspective, it is reasonable to hypothesize that different types of nanopores have different surface properties (*e.g.*, surface charge, roughness, and hydrophilicity), geometry, and membrane stability, corresponding to varying levels of 1/*f* noise. For example, glass nanopores have better hydrophilicity and show less 1/*f* noise than the SiN_x nanopore. SiN_x nanopores are generally fabricated by TEM or focused ion beam (FIB) during which surface roughness, trapped electrons, or ions could be introduced. The low hydrophilicity of the SiN_x surface may produce nanobubbles more easily than biological and glass nanopores, and may produce more pronounced 1/*f* noise. Nanopores based on 2D materials have a higher 1/*f* noise level than other nanopore types, most likely due to mechanical vibrations. In addition, from the dielectric noise perspective, the dielectric loss of the Si substrate would introduce relatively large dielectric noise to SiN_x and 2D material nanopores.

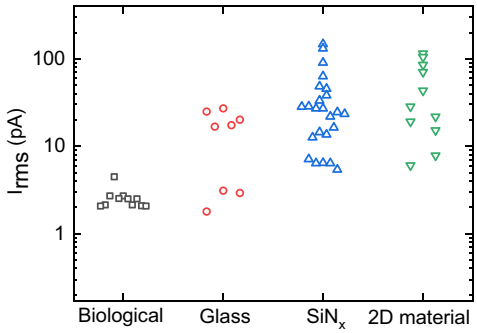

Fig. 7. Comparison of I_{rms} (integrated from 1 Hz to 10 kHz) for different types of nanopores (data from Tables 1–4).

8. Conclusion and future prospects

In summary, we reviewed and summarized the physical models, origins, and reduction methods for four noise components in nanopore sensors (1/*f* noise, white noise, dielectric noise, and amplifier noise). For the first time, we calculated and benchmarked the RMS values for different types of nanopores. There is a clear material-specific noise characteristic for nanopore sensors. Biological and glass nanopores show less RMS noise than SiN_x and 2D material nanopores. There are still many unknowns of nanopore noise. The exact origin of the noise, especially the origin of 1/*f* noise, is still not clear. Without pinpointing the exact noise origins, the noise reduction effort can only be performed by an "error-and-try" approach. We need more theoretical and experimental work in this area. For example, it was previously observed that the nanopore noise can be conditioned by applying an electric field, however, the physical mechanisms of this "conditioning" remain unknown. In addition, we need to develop deeper insight into the impact of nanopore surface properties on the noise performances to control and modify its property. Fabrication methods beyond TEM and FIB may reduce the defect states in the pore-forming material (for reducing the dielectric noise). Lastly, we need to develop high performance, nanopore-integrated amplifiers to reduce the amplifier noise. We anticipate this review article will enhance our understanding of the impact of material properties on the nanopore noise and provide an informative tutorial into developing future nanopore sensors with a high SNR.

Declaration of competing interest

The authors declare that they have no known competing financial interests or personal relationships that could have appeared to influence the work reported in this paper.

Table 4
Noise level statistic of a nanopore based on a 2D material.

Structure	I_{rms}(pA)	Diameter (nm)	Ionic strength (Molar)	pH	Bias (mV)	Ref.
Bare graphene	115.39	4.0	1.0	8.0	100	71
	104.93	10.0	1.0	8.1	100	69
	85.79	8.0	1.0	9.0	100	78
Graphene deposited TiO_2	7.87	7.5	1.0	9.0	100	78
Graphene on quartz	70.45	6.0	1.0	8.0	100	68
Multilayer graphene on quartz	21.80	5.0	1.0	8.0	100	68
h-BN	43.46	n/a	1.0	7.8	n/a	90
	28.55	5.0	1.0	8.0	100	72
h-BN on pyrex	15.26	4.0	1.0	8.0	100	72
h-BNs on pyrex	6.06	8.0	1.0	8.0	100	72
MoS_2	19.15	2.8	0.4	8.0	100	80

Acknowledgments

This work is partially supported by the National Science Foundation under Grant No. 1710831, 1902503, and 1912410. Any opinions, findings, and conclusions or recommendations expressed in this work are those of the authors and do not necessarily reflect the views of the National Science Foundation. This project was also partially supported by National Key Research and Development Program of China (2016YFB0402700), National Key Scientific Instrument and Equipment Development Projects of China (51727901), and China Postdoctoral Science Foundation (2017M620942).

References

1. Clarke J, Wu HC, Jayasinghe L, et al. Continuous base identification for single-molecule nanopore DNA sequencing. Nat Nanotechnol 2009;4(4):265-70.
2. Garaj S, Liu S, Golovchenko JA, et al. Molecule-hugging graphene nanopores. Proc Natl Acad Sci U S A 2013;110(30):12192-6.
3. Plesa C, Kowalczyk SW, Zinsmeester R, et al. Fast translocation of proteins through solid state nanopores. Nano Lett 2013;13(2):658-63.
4. Li JL, Stein D, Qun C, et al. Solid state nanopore as a single DNA molecule detector. Biophys J 2003;84(2):134a-5a.
5. Lua RC, Grosberg AY. First passage times and asymmetry of DNA translocation. Phys Rev E 2005;72(6), 061918.
6. Heins EA, Siwy ZS, Baker LA, et al. Detecting single porphyrin molecules in a conically shaped synthetic nanopore. Nano Lett 2005;5(9):1824-9.
7. Storm AJ, Chen JH, Zandbergen HW, et al. Translocation of double-strand DNA through a silicon oxide nanopore. Phys Rev E 2005;71(5), 051903.
8. Storm AJ, Storm C, Chen JH, et al. Fast DNA translocation through a solid-state nanopore. Nano Lett 2005;5(7):1193-7.
9. Fologea D, Gershow M, Ledden B, et al. Detecting single stranded DNA with a solid state nanopore. Nano Lett 2005;5(10):1905-9.
10. Yan H, Xu BQ. Towards rapid DNA sequencing: detecting single-stranded DNA with a solid-state nanopore. Small 2006;2(3):310-2.
11. Keyser UF, Koeleman BN, Van Dorp S, et al. Direct force measurements on DNA in a solid-state nanopore. Nat Phys 2006;2(7):473-7.
12. Healy K. Nanopore-based single-molecule DNA analysis. Nanomedicine 2007;2(4):459-81.
13. Branton D, Deamer DW, Marziali A, et al. The potential and challenges of nanopore sequencing. Nat Biotechnol 2008;26(10):1146-53.
14. Talaga DS, Li JL. Single-molecule protein unfolding in solid state nanopores. J Am Chem Soc 2009;131(26):9287-97.
15. Wanunu M, Sutin J, Meller A. DNA profiling using solid-state nanopores: detection of DNA-binding molecules. Nano Lett 2009;9(10):3498-502.
16. Wanunu M, Morrison W, Rabin Y, et al. Electrostatic focusing of unlabelled DNA into nanoscale pores using a salt gradient. Nat Nanotechnol 2010;5(2):160-5.
17. Venkatesan BM, Bashir R. Nanopore sensors for nucleic acid analysis. Nat Nanotechnol 2011;6(10):615-24.
18. Wei RS, Gatterdam V, Wieneke R, et al. Stochastic sensing of proteins with receptor-modified solid-state nanopores. Nat Nanotechnol 2012;7(4):257-63.
19. Lin Y, Ying YL, Shi X, et al. Direct sensing of cancer biomarkers in clinical samples with a designed nanopore. Chem Commun 2017;53(84):11564-7.
20. Sha J, Si W, Xu B, et al. Identification of spherical and nonspherical proteins by a solid-state nanopore. Anal Chem 2018;90(23):13826-31.
21. Goto Y, Yanagi I, Matsui K, et al. Identification of four single-stranded DNA homopolymers with a solid-state nanopore in alkaline CsCl solution. Nanoscale 2018;10(44):20844-50.
22. Yang H, Li Z, Si W, et al. Identification of single nucleotides by a tiny charged solid-state nanopore. J Phys Chem B 2018;122(32):7929-35.
23. Bello J, Mowla M, Troise N, et al. Increased dwell time and occurrence of dsDNA translocation events through solid state nanopores by LiCl concentration gradients. Electrophoresis 2019;40(7):1082-90.
24. Wang J, Yang J, Ying YL, et al. Nanopore-based confined spaces for single-molecular analysis. Chem Asian J 2018;14(3):389-97.
25. Rivas F, Zahid OK, Reesink HL, et al. Label-free analysis of physiological hyaluronan size distribution with a solid-state nanopore sensor. Nat Commun 2018;9(1):1037.
26. Plesa C, Verschueren D, Pud S, et al. Direct observation of DNA knots using a solid-state nanopore. Nat Nanotechnol 2016;11(12):1093-7.
27. Yusko EC, Bruhn BR, Eggenberger OM, et al. Real-time shape approximation and fingerprinting of single proteins using a nanopore. Nat Nanotechnol 2017;12(4):360-7.
28. Kasianowicz JJ, Brandin E, Branton D, et al. Characterization of individual polynucleotide molecules using a membrane channel. Proc Natl Acad Sci U S A 1996;93(24):13770-3.
29. Derrington IM, Butler TZ, Collins MD, et al. Nanopore DNA sequencing with MspA. Proc Natl Acad Sci U S A 2010;107(37):16060-5.
30. Jain M, Olsen HE, Paten B, et al. The Oxford Nanopore MinION: delivery of nanopore sequencing to the genomics community. Genome Biol 2016;17(1):239.
31. Jain M, Koren S, Miga KH, et al. Nanopore sequencing and assembly of a human genome with ultra-long reads. Nat Biotechnol 2018;36(4):338-45.
32. Albrecht T. Single-molecule analysis with solid-state nanopores. Annu Rev Anal Chem 2019;12(1):371-87.
33. Lee K, Park KB, Kim HJ, et al. Recent progress in solid-state nanopores. Adv Mater 2018;30(42), 1704680.
34. Li J, Stein D, McMullan C, et al. Ion-beam sculpting at nanometre length scales. Nature 2001;412(6843):166-9.
35. Roshan KA, Tang Z, Guan W. High fidelity moving Z-score based controlled breakdown fabrication of solid-state nanopore. Nanotechnology 2019;30(9), 095502.
36. Chen W, Liu G-C, Ouyang J, et al. Graphene nanopores toward DNA sequencing: a review of experimental aspects. SCIENCE CHINA Chem 2017;60(6):721-9.
37. Zhang SD, Li MZ, Su B, et al. Fabrication and use of nanopipettes in chemical analysis. Annu Rev Anal Chem 2018;11(1):265-86.
38. Mara A, Siwy Z, Trautmann C, et al. An asymmetric polymer nanopore for single molecule detection. Nano Lett 2004;4(3):497-501.
39. Tabard-Cossa V, Trivedi D, Wiggin M, et al. Noise analysis and reduction in solid-state nanopores. Nanotechnology 2007;18(30), 305505.
40. Manrao EA, Derrington IM, Laszlo AH, et al. Reading DNA at single-nucleotide resolution with a mutant MspA nanopore and phi29 DNA polymerase. Nat Biotechnol 2012;30(4):349-53.
41. Nouri R, Tang ZF, Guan WH. Calibration-free nanopore digital counting of single molecules. Anal Chem 2019;91(17):11178-84.
42. Schneider GF, Xu Q, Hage S, et al. Tailoring the hydrophobicity of graphene for its use as nanopores for DNA translocation. Nat Commun 2013;4(1):2619.
43. Uram JD, Ke K, Mayer M. Noise and bandwidth of current recordings from submicrometer pores and nanopores. ACS Nano 2008;2(5):857-72.
44. Smeets RMM, Keyser UF, Dekker NH, et al. Noise in solid-state nanopores. Proc Natl Acad Sci U S A 2008;105(2):417-21.
45. Smeets RMM, Dekker NH, Dekker C. Low-frequency noise in solid-state nanopores. Nanotechnology 2009;20(9), 095501.
46. Hoogerheide DP, Garaj S, Golovchenko JA. Probing surface charge fluctuations with solid-state nanopores. Phys Rev Lett 2009;102(25), 256804.
47. Parkin WM, Drndic M. Signal and noise in FET-nanopore devices. ACS Sens 2018;3(2):313-9.
48. Albu M, Heydt GT. On the use of RMS values in power quality assessment. IEEE Trans Power Delivery 2003;18(4):1586-7.
49. Dutta P, Horn PM. Low-frequency fluctuations in solids: 1/f noise. Rev Mod Phys 1981;53(3):497-516.
50. Hartel AJW, Shekar S, Ong P, et al. High bandwidth approaches in nanopore and ion channel recordings - a tutorial review. Anal Chim Acta 2019;1061:13-27.
51. Siwy Z, Fulinski A. 1/*f* noise in ion transport through nanopores: origins and mechanism. In: Bezrukov SM, ed. Unsolved problems of noise and fluctuations. Melville: Amer Inst Physics; 2003. p. 273-82.
52. Dimitrov V, Mirsaidov U, Wang D, et al. Nanopores in solid-state membranes engineered for single molecule detection. Nanotechnology 2010;21(6), 065502.
53. Rosenstein JK, Wanunu M, Merchant CA, et al. Integrated nanopore sensing platform with sub-microsecond temporal resolution. Nat Methods 2012;9(5):487-92.
54. Lee MH, Kumar A, Park KB, et al. A low-noise solid-state nanopore platform based on a highly insulating substrate. Sci Rep 2014;4:7448.
55. Waggoner PS, Kuan AT, Polonsky S, et al. Increasing the speed of solid-state nanopores. J Vac Sci Technol B 2011;29(3), 032206.
56. Van Der Ziel A. On the noise spectra of semi-conductor noise and of flicker effect. Physica 1950;16(4):359-72.
57. Costanzi BN, Dahlberg ED. Emergent 1/f noise in ensembles of random telegraph noise oscillators. Phys Rev Lett 2017;119(9), 097201.
58. Powell MR, Vlassiouk I, Martens C, et al. Nonequilibrium 1/f noise in rectifying nanopores. Phys Rev Lett 2009;103(24), 248104.
59. Fragasso A, Pud S, Dekker C. 1/*f* noise in solid-state nanopores is governed by access and surface regions. Nanotechnology 2019;30(39):395202.
60. Siwy Z, Fulinski A. Origin of 1/*f*(alpha) noise in membrane channel currents. Phys Rev Lett 2002;89(15), 158101.
61. Bezrukov SM, Winterhalter M. Examining noise sources at the single-molecule level: 1/f noise of an open maltoporin channel. Phys Rev Lett 2000;85(1):202-5.
62. Smeets RMM, Keyser UF, Wu MY, et al. Nanobubbles in solid-state nanopores. Phys Rev Lett 2006;97(8), 088101.
63. Roth R, Gillespie D, Nonner W, et al. Bubbles, gating, and anesthetics in ion channels. Biophys J 2008;94(11):4282-98.
64. Beamish E, Kwok H, Tabard-Cossa V, et al. Precise control of the size and noise of solid-state nanopores using high electric fields. Nanotechnology 2012;23(40), 405301.
65. Tasserit C, Koutsioubas A, Lairez D, et al. Pink noise of ionic conductance through single artificial nanopores revisited. Phys Rev Lett 2010;105(26), 260602.
66. Gravelle S, Netz RR, Bocquet L. Adsorption kinetics in open nanopores as a source of low-frequency noise. Nano Lett 2019;19(10):7265-72.
67. Radenovic A, Trepagnier E, Csencsits R, et al. Fabrication of 10 nm diameter hydrocarbon nanopores. Appl Phys Lett 2008;93(18), 183101.
68. Kumar A, Park KB, Kim HM, et al. Noise and its reduction in graphene based nanopore devices. Nanotechnology 2013;24(49), 495503.
69. Heerema SJ, Schneider GF, Rozemuller M, et al. 1/f noise in graphene nanopores. Nanotechnology 2015;26(7), 074001.
70. Arjmandi-Tash H, Belyaeva LA, Schneider GF. Single molecule detection with graphene and other two-dimensional materials: nanopores and beyond. Chem Soc Rev 2016;45(3):476-93.
71. Zhang ZY, Deng YS, Tian HB, et al. Noise analysis of monolayer graphene nanopores. Int J Mol Sci 2018;19(9):2639.
72. Park KB, Kim HJ, Kim HM, et al. Noise and sensitivity characteristics of solid-state nanopores with a boron nitride 2-D membrane on a pyrex substrate. Nanoscale 2016;8(10):5755-63.

73. Bezrukov SM, Kasianowicz JJ. Current noise reveals protonation kinetics and number of ionizable sites in an open protein ion channel. Phys Rev Lett 1993;70(15):2352-5.
74. Wen C, Zeng SS, Arstila K, et al. Generalized noise study of solid-state nanopores at low frequencies. ACS Sens 2017;2(2):300-7.
75. Perry D, Momotenko D, Lazenby RA, et al. Characterization of nanopipettes. Anal Chem 2016;88(10):5523-30.
76. Steinbock LJ, Bulushev RD, Krishnan S, et al. DNA translocation through low-noise glass nanopores. ACS Nano 2013;7(12):11255-62.
77. Powell MR, Martens C, Siwy ZS. Asymmetric properties of ion current 1/f noise in conically shaped nanopores. Chem Phys 2010;375(2):529-35.
78. Merchant CA, Healy K, Wanunu M, et al. DNA translocation through graphene nanopores. Nano Lett 2010;10(8):2915-21.
79. Chen P, Mitsui T, Farmer DB, et al. Atomic layer deposition to fine-tune the surface properties and diameters of fabricated nanopores. Nano Lett 2004;4(7):1333-7.
80. Waduge P, Bilgin I, Larkin J, et al. Direct and scalable deposition of atomically thin low-noise MoS_2 membranes on apertures. ACS Nano 2015;9(7):7352-9.
81. Saleh OA, Sohn LL. Quantitative sensing of nanoscale colloids using a microchip Coulter counter. Rev Sci Instrum 2001;72(12):4449-51.
82. Balan A, Machielse B, Niedzwiecki D, et al. Improving signal-to-noise performance for DNA translocation in solid-state nanopores at MHz bandwidths. Nano Lett 2014;14(12):7215-20.
83. Choi W, Jeon ES, Chun KY, et al. A low-noise silicon nitride nanopore device on a polymer substrate. PLoS One 2018;13(7), e0200831.
84. de Vreede LJ, Ying CF, Houghtaling J, et al. Wafer-scale fabrication of fused silica chips for low-noise recording of resistive pulses through nanopores. Nanotechnology 2019;30(26), 265301.
85. Sze JYY, Kumar S, Ivanov AP, et al. Fine tuning of nanopipettes using atomic layer deposition for single molecule sensing. Analyst 2015;140(14):4828-34.
86. Mohammad MM, Iyer R, Howard KR, et al. Engineering a rigid protein tunnel for biomolecular detection. J Am Chem Soc 2012;134(22):9521-31.
87. Soskine M, Biesemans A, Moeyaert B, et al. An engineered ClyA nanopore detects folded target proteins by selective external association and pore entry. Nano Lett 2012;12(9):4895-900.
88. Freedman KJ, Otto LM, Ivanov AP, et al. Nanopore sensing at ultra-low concentrations using single-molecule dielectrophoretic trapping. Nat Commun 2016;7(1), 10217.
89. Janssen XJ, Jonsson MP, Plesa C, et al. Rapid manufacturing of low-noise membranes for nanopore sensors by trans-chip illumination lithography. Nanotechnology 2012;23(47), 475302.
90. Zhou Z, Hu Y, Wang H, et al. DNA translocation through hydrophilic nanopore in hexagonal boron nitride. Sci Rep 2013;3:3287.